

Cite this: *J. Mater. Chem. A*, 2020, **8**, 16582

Enhancing metal–support interaction by *in situ* ion-exchanging strategy for high performance Pt catalysts in hydrogen evolution reaction†

Xulei Sui,^{ab} Lei Zhang,^b Junjie Li,^b Kieran Doyle-Davis,^b Ruying Li,^b Zhenbo Wang^{*a} and Xueliang Sun^{†b}

Metal–support interaction (MSI) holds great promise for the development of heterogeneous catalysts. Accordingly, it is essential to implement facile methods to modulate MSI for the improvement of catalytic performance. In this study, an effective method is proposed to directly enhance MSI, wherein the electronic properties of Pt are altered by the ion-exchanging reaction of the support, affording incredible catalytic performance. Pt nanoparticles with 1.5 nm diameters are successfully deposited on a quasi-layered sodium titanate support *via* atomic layer deposition (ALD). The ion-exchanging reaction of the support between the Na-ions and H-ions in acidic media results in the transformation of the support structure, and further modulates the Pt local electronic structure. Such behaviour facilitates the enhancement of MSI offering highly active and stable Pt sites. The as-prepared catalyst exhibits much higher mass activity and long-term stability for the hydrogen evolution reaction (HER) in comparison with Pt/TiO₂ and commercial Pt/C. The enhancement mechanism of MSI comes through the structural variation of the support, with modified charge transfer between the Pt and its support. Moreover, this new approach provides a facile and reliable path to develop advanced catalysts with enhanced MSI and motivates further research in many fields.

Received 7th March 2020
Accepted 16th July 2020

DOI: 10.1039/d0ta02681f

rsc.li/materials-a

Introduction

Noble metal Pt has shown considerably high catalytic activity for many important reactions, such as the hydrogen evolution reaction (HER) and oxygen reduction reaction (ORR), compared to other metals.^{1–3} Owing to the limited reserves of Pt metal, reducing the amount of Pt used without a reduction in catalytic performance is of the utmost importance. Much of the current research in the field is focused on this topic.^{4–6} One important direction is to improve the Pt utilization rate by decreasing the Pt particle size since the catalytic reactions occur mainly on the catalyst surface. One new approach is Pt single atom catalysis, which allows for maximum atomic utilization and improved exposure of the active sites.^{6–8} A wide variety of synthesis methods and applications for single atom Pt have been developed.⁹ The other direction is to improve the activity of Pt sites through a modification of the Pt electronic structure. The

modulation of Pt strain is an important approach in developing highly active Pt sites. Pt alloying and support regulation are two promising methods to realize Pt strain.^{10–12} Additionally, the important role of the MSI has also been studied for the improvement of catalytic activity and stability by tuning the Pt electronic structure.^{13–16} Many supports have been identified to enable interaction with Pt, such as metal oxides,^{16–18} carbides¹⁹ and nitrides.²⁰ Among them, titanium oxide is the most frequently used substrate due to its ability to withstand corrosion in harsh conditions, its environmental friendliness, and its low cost. Lately, sodium titanate as a Pt support has attracted a lot of attention as it can adjust the interface interaction, due to its abundant surface defects, drastically enhancing Pt catalytic performance.²¹

Recently, control of the MSI has emerged as an effective strategy in improving catalytic performance. MSI tuning strategies have been extensively studied and developed, including possible synthesis methods, control of both the support and metal, and post-treatment strategies.²² ALD is one such method to greatly enhance the MSI, where the deposition of an initial layer of atoms can be embedded into the surface of the support, ensuring a stronger MSI than conventional chemical methods.²³ The metal particle size is another important factor for MSI modulation. Recent research shows that the MSI is most impactful for metal nanoparticles smaller than 4 nm.^{24,25} Moreover, the MSI can be modulated by altering the

^aMIT Key Laboratory of Critical Materials Technology for New Energy Conversion and Storage, School of Chemistry and Chemical Engineering, State Key Laboratory of Urban Water Resource and Environment, Harbin Institute of Technology, 150001, China. E-mail: wangzhib@hit.edu.cn

^bDepartment of Mechanical and Materials Engineering, University of Western Ontario, London, ON N6A 5B9, Canada. E-mail: xsun9@uwo.ca

† Electronic supplementary information (ESI) available. See DOI: 10.1039/d0ta02681f

composition and morphology of the supports.^{26–28} It is worth noting that post-treatment strategies allow the direct tuning of the MSI on the original catalysts. Therefore, the post-treatment strategies are very critical. Currently, most post-treatment strategies require complicated processing, such as heat treatment, reduction–oxidation reaction or overlayer deposition,^{29–32} which are likely to lead to the loss of active sites of the supported metal due to the aggregation of nanoparticles or the surface coating. Accordingly, the development of a facile post-treatment strategy capable of tuning the MSI is highly desirable without the loss of active sites.

Herein, we propose a facile *in situ* ion-exchanging strategy to directly enhance the MSI between Pt and titanium oxide and promote its electrocatalytic performance for HER in acidic environments. Quasi-layered sodium titanate (NaTiO) nanowires are used as the support for the deposition of Pt nanoparticles by ALD. As NaTiO is isostructural with titanite hydroxide, the interlayer Na-ions can easily exchange with H-ions in acidic environments, resulting in the broadening of the lattice spacing. The structural change of the support further induces an electronic change in the Pt–support environment, leading to a more readily reduced Pt oxidation state. The enhanced MSI dramatically improves the activity and stability of Pt sites. Accordingly, the Pt/NaTiO catalyst shows greatly enhanced HER activity and durability compared with that of Pt/TiO₂ and commercial Pt/C.

Results and discussion

The motivation of utilizing titanium oxide as a Pt support is its durable electrochemical corrosion resistance and the metal–support interaction (MSI), resulting in improved electrocatalytic activity and durability of Pt.^{33–35} The synthesis procedure of Pt deposited on NaTiO and TiO supports is schematically illustrated in Fig. 1, including the synthesis of the support and the deposition of Pt. Na₂Ti₂O₅·H₂O nanowires were prepared *via* a facile hydrothermal process. The TiO support was obtained *via* a protonation process and a sintering process, wherein an ion-exchanging reaction between Na-ions and H-ions took place. As for the NaTiO support, a similar process was used, but the

protonation process was excluded. Finally, ALD was employed to deposit Pt metal on TiO and NaTiO supports. The phase structures of Pt-based catalysts were explored by X-ray diffraction (XRD) and are shown in Fig. S1.† As observed, all diffraction peaks of Pt/TiO can be assigned to the anatase phase of TiO₂ (JCPDS No. 21-1272). According to our previous work,^{36–38} Na₂Ti₂O₅·H₂O can be converted into H₂Ti₂O₅·H₂O during the protonation process, and then the decomposition reaction under high temperature results in a pure TiO₂ crystal phase. In contrast, Pt/NaTiO exhibits a completely different structure with an approximate body-centre orthorhombic structure of H₂Ti₂O₅·H₂O (JCPDS No. 47-0124), which displays a layered structure. Due to the partial Na loss during water washing for NaTiO, its chemical composition is not the same as Na₂Ti₂O₅, and its X-ray diffraction peaks appear to shift. The shift of peak (200) to higher angles indicates that the interlayer spacing shrinks, which is mainly due to the insertion of Na-ions and the complete loss of crystallographic water in the interlayers.³⁸ The presence of Na-ions is visible in the elemental mapping, as displayed in Fig. S2,† and the atom percent of Na is about 6.8% as demonstrated in the energy dispersive spectroscopy (EDS) provided below. However, the Pt diffraction peak and elemental signal are very difficult to observe, which may be due to the extremely low Pt content. The inductively coupled plasma-optical emission spectrometry (ICP-OES) can directly verify the presence of Pt, and the actual Pt mass contents of Pt/NaTiO and Pt/TiO catalysts are respectively about 0.23 wt% and 0.16 wt%. The ultralow Pt content obtained through ALD is beneficial for increasing the Pt utilization and enhancing the MSI.

Generally, one-dimensional (1D) structures are beneficial for increasing the performance of electrocatalysts, which has been emphasized by numerous researchers, driving our decision in the use of a 1D support.^{39–41} As shown in Fig. S3† and 2, the 1D nanowire morphology of the as-prepared catalysts can be visibly observed, and some crossing nanowires occur to gather into bunches. In addition, the protonation process has no influence on the 1D structure for Pt/TiO compared with Pt/NaTiO. The diameters of the nanowires are approximately 50 nm, and the length of nanowires are about 2 μm. High-resolution transmission electron microscopy (HRTEM) images of TiO and NaTiO are further examined to confirm the phase structures of the supports. As shown in the inset of Fig. 2a, the lattice fringes of about 0.48 nm and 0.35 nm can be clearly seen, corresponding to the crystal planes of (002) and (101) of anatase TiO₂, respectively. In the case of NaTiO, the lattice fringes of about 0.62 nm and 0.36 nm in the inset of Fig. 2b reveal the lattice planes of (200) and (110) of quasi-layered NaTiO. These observations are consistent with the XRD measurements.

The ultralow Pt content seriously limits the direct observation of Pt nanoparticles (NPs). From TEM and HRTEM images, it is quite difficult to distinguish ultrafine Pt nanoparticles from the titanium oxide substrate. Hence, scanning transmission electron microscopy (STEM) with a high-angle annular dark field detector (HAADF) was employed to observe the morphology of Pt deposited on the support. As shown in Fig. 2c and d, many highlighted dots are homogeneously dispersed on the nanowire supports, which can be identified as Pt NPs. The

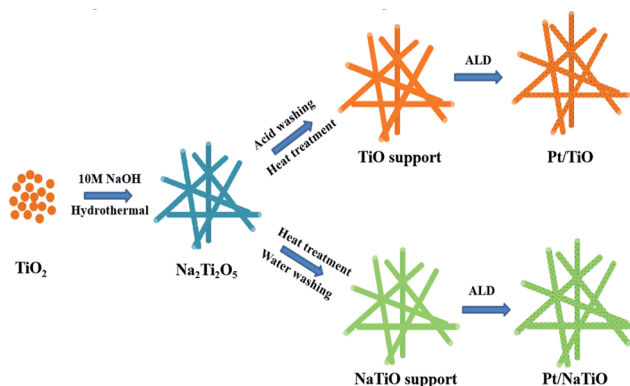


Fig. 1 Schematic of the synthesis process of Pt/TiO and Pt/NaTiO catalysts.

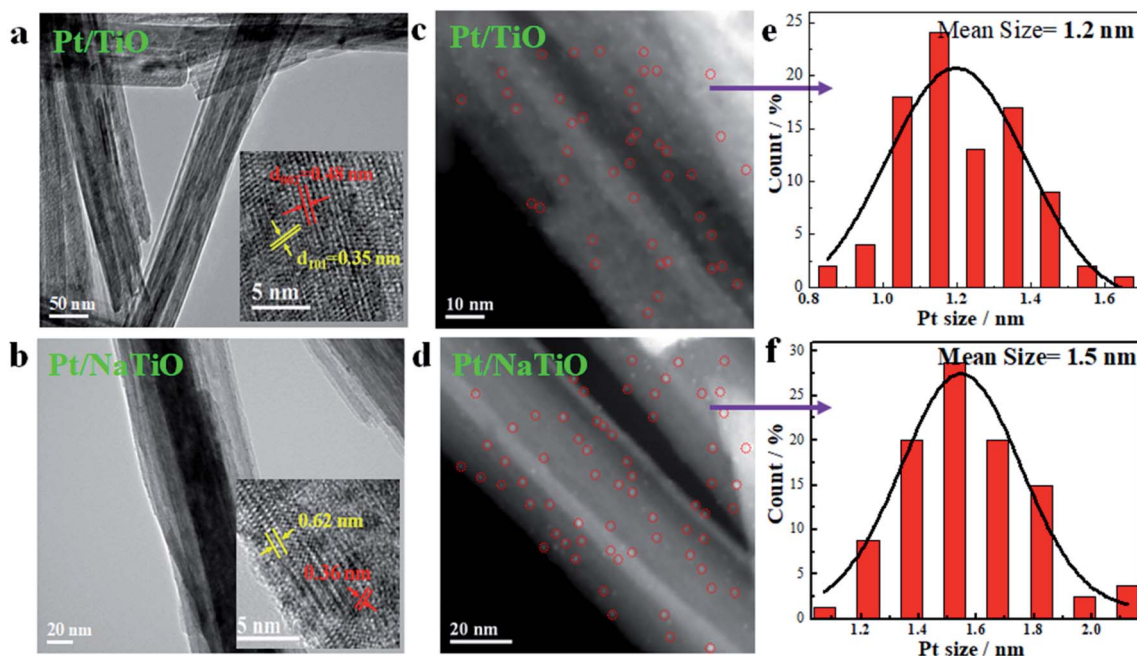


Fig. 2 The morphology characterization of Pt/TiO and Pt/NaTiO catalysts. (a and b) TEM images of Pt/TiO and Pt/NaTiO catalysts, the inserts are the related HRTEM images. (c and d) HAADF-STEM images of Pt/TiO and Pt/NaTiO catalysts and the related statistics of Pt size (e and f).

sizes of Pt NPs on TiO and NaTiO are respectively around 1–2 nm with a narrow size distribution. According to their size statistics in Fig. 2e and f, the average size of Pt NPs on NaTiO are about 1.5 nm, which is slightly bigger than that on TiO (1.2 nm), which is consistent with its higher Pt content by ICP. The above results strongly support the successful deposition of ultrafine Pt NPs on 1D nanowires supports with uniform distribution. The ultrafine Pt size results in the appreciably abundant active sites enabling increased catalytic activity and Pt utilization. Additionally, using ALD to deposit ultrafine Pt NPs directly on the support enables an improved MSI at the atomic level, resulting in the improved activity and stability of Pt catalysts.²³

X-ray absorption spectroscopy (XAS) was utilized to further study the local electronic structure of Pt NPs for both Pt catalysts. Pt foil is also analyzed for comparison. Fig. 3 shows the normalized X-ray absorption near edge structure (XANES) spectra for both Pt L_{3-} and L_{2-} edges of the ultrafine Pt NPs. The

whiteline (WL) in Pt L_{2} and L_{3} edges can be attributed to the dominant $2p_{1/2}$ and $2p_{3/2}$ transition to $5d_{3/2}$ and $5d_{5/2,3/2}$, respectively, reflecting the unoccupied densities of states of Pt $5d_{5/2}$ and $5d_{3/2}$ character in the samples.²³ Due to the large spin-orbit coupling of the Pt 5d orbitals, the Pt L_{3-} and L_{2-} edge WLs should be used together to analyze the electronic structure of the samples.⁴² As shown in Fig. 3, the WL peaks of the Pt L_{3} and L_{2} edges for Pt/NaTiO and Pt/TiO catalysts both exhibit higher intensity and a similar right-shift compared with that of Pt foil, indicating their higher unoccupied densities of 5d states. This illustrates that Pt NPs on NaTiO and TiO supports are partially oxidized, which is detrimental to their catalytic activities. It is generally hypothesized that the Pt oxidation mainly originates from the binding of oxygen-containing species on the Pt surface, and the oxidation degree depends on the specific surface area of Pt and the binding strength of oxygen-containing species on Pt. Therefore, the abundant oxidation of Pt/NaTiO and Pt/TiO catalysts should result from the abundant specific surface of Pt NPs due to their smaller Pt sizes. Close examination reveals that the intensity of the Pt L_{3} and L_{2} WL peaks still exhibits obvious differences for Pt/NaTiO and Pt/TiO catalysts. The lower intensity of the WL peak for the Pt/NaTiO catalyst implies the more reduced Pt state, which can be attributed to the larger Pt size due to the higher Pt content of Pt/NaTiO.

The electrocatalytic performance of as-prepared catalysts for the hydrogen evolution reaction (HER) was measured using a rotating-disk electrode (RDE) in 0.1 M HClO₄ electrolyte, where the commercial Pt/C (10 wt%, Johnson Matthey) was also included for comparison. To avoid confusion, the catalysts tested in acidic electrolyte were recorded as Pt/H-NaTiO and Pt/TiO catalysts.

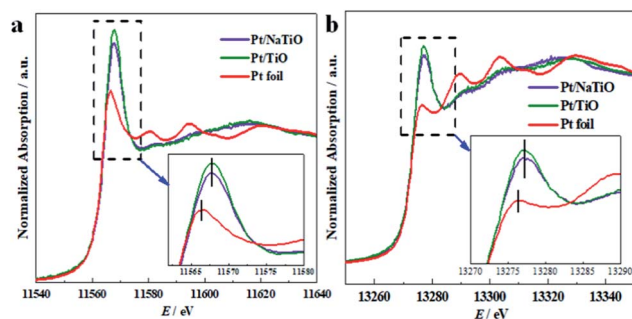


Fig. 3 XANES spectra for Pt L_{3-} (a) and L_{2-} (b) edges for Pt/NaTiO and Pt/TiO catalysts.

H-TiO. As shown in Fig. 4a, the as-prepared catalysts exhibit excellent catalytic activity towards the HER with negligible overpotential, which is similar to commercial Pt/C. In sharp contrast, both pure supports of H-NaTiO and H-TiO exhibit no activity, indicating that the high HER activities of the as-prepared Pt-based catalysts result from the Pt metal. More importantly, the Pt/H-NaTiO catalyst shows higher HER activity than Pt/H-TiO with higher current density. Tafel curves plotted in Fig. 4b show consistent results with the polarization curves. The commercial Pt/C achieves the smallest Tafel slope of 29 mV dec^{-1} , as the Pt/H-NaTiO and Pt/H-TiO catalysts exhibit the slightly larger Tafel slopes of 38 and 43 mV dec^{-1} , respectively. Furthermore, as presented in Fig. S4,[†] the hydrogen absorption/desorption peaks of Pt are negligible due to the ultralow Pt loading. It is too complex to normalize the current by the Pt electrochemical active surface area (ECSA). Thus, we normalized the current density by the Pt mass. As shown in Fig. 4c and d, the polarization curves exhibit that Pt/H-NaTiO and Pt/H-TiO catalysts have much higher mass activity compared with commercial Pt/C. The mass activities of the HER for Pt/H-NaTiO and Pt/H-TiO catalysts at the overpotential of 50 mV are respectively 10.3 and 8.8 A mg^{-1} , much higher than 0.4 A mg^{-1} of commercial Pt/C. Such a high mass activity of Pt/NaTiO for HER is also prominent compared to the other state-of-the-art Pt-based electrocatalysts reported recently, and even superior to some Pt single-atom catalysts in the literature, as listed in Table S1.[†] The ultrahigh catalytic efficiency of Pt is quite meaningful for practical application. The small Pt NP size for the as-prepared catalysts should be one of the important factors leading to their high catalytic activities due to their high Pt atom utilization. When increasing the size of Pt NPs by increasing the

Pt ALD time, the Pt/H-NaTiO catalyst presents the lower mass activity, as shown in Fig. S5,[†] verifying the Pt size effect on catalytic performance. Strikingly, the mass activity of Pt/H-NaTiO is slightly higher than that of Pt single atoms and clusters supported on graphene nanosheets by ALD in our previous work (10.1 A mg^{-1} in $0.5 \text{ M H}_2\text{SO}_4$).⁴² Accordingly, the MSI between Pt and titanium oxide supports should be another important factor of HER improvement. The MSI can increase the electronic density on Pt, leading to the reduction of the oxidation state of the Pt NPs, and further improving the H-ion adsorption and reduction.

More interestingly, Pt/NaTiO shows lower catalytic activity than Pt/TiO in neutral electrolyte (1 M NaCl), as shown in Fig. S6,[†] which can be attributed to the Pt size effect. On the contrary, Pt/H-NaTiO exhibits enhanced HER activity compared to Pt/H-TiO in acidic electrolyte, as presented in Fig. 4c and d. Therefore, the Pt size effect cannot explain it. The changes of the electronic structure of Pt/H-NaTiO should be responsible for this phenomenon. This result probably illustrates that the Pt/H-NaTiO catalyst demonstrates an enhanced MSI compared to the Pt/H-TiO catalyst.

Furthermore, the long-term stability of Pt/H-NaTiO and Pt/H-TiO catalysts in acidic electrolyte were examined by cycling continuously between 0 V and -0.3 V for 10 000 cycles. The polarization curves before and after 10 000 cycles for all catalysts are shown in Fig. 4e, f and S7.[†] It can be observed that after 10 000 cycles, the Pt/H-NaTiO catalyst provides similar activity as the uncycled catalyst, with a negligible loss of current density. Comparatively, Pt/H-TiO and commercial Pt/C catalysts show a visible loss of current densities. The mass activities for all catalysts at 50 mV overpotential after 10 000 cycles were also

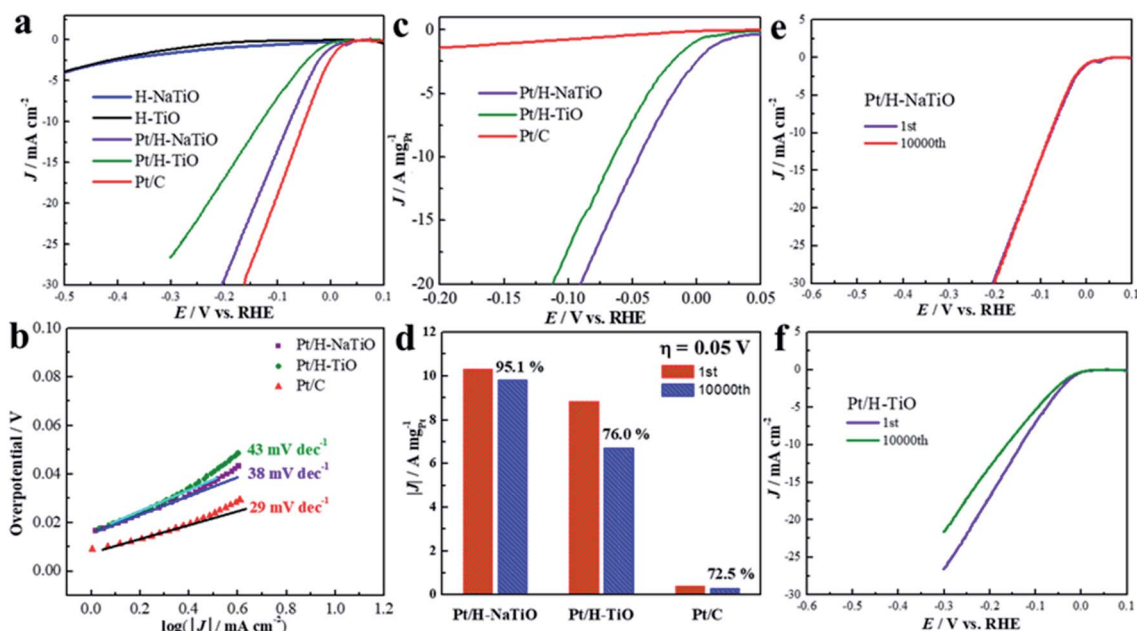


Fig. 4 Electrochemical performance of the HER for Pt/NaTiO, Pt/TiO and commercial Pt/C in 0.1 M HClO_4 . (a) HER polarization curves normalized by electrode area; (b) Tafel curves; (c) HER polarization curves normalized by Pt mass; (d) the related activity and stability at overpotential 50 mV; (e and f) HER stability after 10 000 cycles.

calculated and shown in Fig. 4c. The Pt/H-NaTiO catalyst retains around 95.1% of its initial activity, which is significantly higher than the Pt/H-TiO catalyst (76.0%) and commercial Pt/C (72.5%). To further understand the phenomenon, TEM was performed to study the morphology of Pt NPs after the stability test. It can be obviously seen from Fig. S8† that after 10 000 cycles, the Pt size of the Pt/H-NaTiO catalyst is unchanged while the Pt size of Pt/H-TiO increases from 1.2 nm to 1.5 nm. The dissolution and reduction of Pt during cycling is mainly responsible for the increase of Pt size, further resulting in the catalytic performance degradation. The Pt oxidation state is beneficial for its dissolution. The MSI can increase the electronic density on Pt, leading to the reduction of the oxidation state of the Pt NPs, and further improve its acid-resistance behaviour. Therefore, the superior stability of the Pt/H-NaTiO catalyst identifies the stronger MSI between Pt NPs and the substrate in comparison with that of Pt/H-TiO.

In order to confirm and explore the origin of the enhanced MSI of the Pt/H-NaTiO catalyst, the changes of both substrate and Pt in acidic solution (test environment) were further investigated. Pt/H-TiO and Pt/H-NaTiO samples were obtained after acidic treatment for 3 h. Firstly, the phase structure was characterized by XRD, as shown in Fig. S9.† As expected, Pt/H-TiO displays the same phase structure of anatase TiO₂ with Pt/TiO. This illustrates that the acidic treatment has no influence on the phase structure of Pt/TiO, which can be attributed to the excellent chemical stability of anatase TiO₂ in acidic solution. According to the EDS results (Fig. S10 and Table S2†), the atomic ratio of Ti and O for Pt/TiO and Pt/H-TiO are both about 0.34, further confirming the invariant ingredients of Pt/TiO during the acidic treatment. As for the Pt/NaTiO catalyst, significant changes in both the component and phase structure can be observed after the acidic treatment. The EDS and XRD patterns of Pt/H-NaTiO are displayed in Fig. 5a and b. As observed, the atomic ratio of Na/Ti in Pt/H-NaTiO is only 0.13, much lower than that of Pt/NaTiO (0.28), indicating that the majority of Na-ions are extracted by H-ions during the acidic treatment. Meanwhile, the XRD pattern of Pt/H-NaTiO is nearly the same as the diffraction pattern of Pt/NaTiO but with a shift toward lower angles of peak (200), as displayed in the enlarged XRD in Fig. 5b. According to the Debye–Scherrer formula, the left-shift of peak (200) demonstrates the larger lattice interlayer spacing of (200). The result can be ascribed to the ion-exchanging reaction between Na-ions and H-ions during the protonation process. Similar results have been previously reported by our group.³⁷ Such phenomena can also be obviously observed in the HRTEM images, as shown in Fig. 5c. In order to accurately obtain the inter-planar spacing of d_{200} of the NaTiO support before and after the protonation process, the distances of 8–9 interlayer spacing (red line in Fig. 5c) are measured, and then the average can be calculated. As presented, the significant increase of the lattice plane spacing of (200) for NaTiO can be observed after the protonation process, from 0.62 nm to 0.72 nm. This result is in good agreement with the characterization of XRD. All the above investigation clarifies that in an acidic environment, the Pt/NaTiO catalyst would go through a protonation process resulting in the change of phase structure

of the support, while the Pt/TiO catalyst remains substantially unchanged.

Through the above investigation, it can be inferred that the transformation of the phase structure of the NaTiO support in an acidic environment should be responsible for the enhanced MSI between Pt and support. To validate our speculation, the morphology and electronic structure of Pt NPs were further studied for Pt/H-NaTiO after a protonation process by HAADF-STEM and XAS. As shown in Fig. S11,† the dispersion of Pt NPs on the support after acidic treatment is still very uniform as before. Through the size statistics, a Pt average size of 1.5 nm is the same with that of Pt/NaTiO, suggesting that the protonation process has little influence on the morphology of Pt NPs. However, the change of Pt electronic structure can be easily found from the XAS results in Fig. 6. As observed in the normalized XANES spectra at the Pt L₃-edge (Fig. 6a), after the ion-exchanging reaction of the support, the Pt L₃-edge WL peak of Pt/H-NaTiO catalyst shows a small left-shift, and the intensity of the WL peak decreases significantly. This implies that the electronic density on Pt NPs increased. Furthermore, the WL peak of the corresponding Pt L₂-edge shows similar variation compared with that of the Pt L₃-edge, as displayed in Fig. 6b. It can be concluded from the changes of both Pt L₃- and L₂-edge WLs that the Pt NPs of Pt/H-NaTiO present more metallic nature compared with that of Pt/NaTiO. In other words, the Pt local electronic density of Pt/H-NaTiO catalyst increases after acid treatment. Due to the consistent Pt NP size before and after acid treatment, the more reduced state of Pt NPs demonstrates a weaker binding of oxygen-containing species. The change of binding strength can be visibly observed from the Pt L₃-edge extended X-ray absorption fine structure (EXAFS) Fourier transformed (FT) spectra (Fig. S12†). The longer Pt–O bond after acid treatment corresponds to the weaker Pt–O binding, implying the change of MSI between Pt and support, which can be attributed to the change of the support phase structure during the protonation process. Undoubtedly, the enhanced MSI of the Pt/H-NaTiO catalyst in an acidic environment can be verified. The resulting increased metallic state of Pt NPs is responsible for the observed increase of HER activity and stability for the Pt/H-NaTiO catalyst.

The interaction mechanism should be further discussed to clarify the origin of the enhanced MSI. The change in electronic properties of Pt on a titanium oxide substrate due to MSI has been extensively confirmed and attributed to the overlapping of the occupied d orbitals of Pt and the unoccupied d orbitals of titanium oxide.⁴³ The increased electronic density of Pt originates not only from the charge transfer from the support to Pt, but also from the alloy formation between Pt and the oxide support.⁴⁴ Namely, the MSI is based on the interplay between the Pt and oxide support, which is tightly associated with their morphology and structure. For our system, as displayed in Fig. 6c, during the protonation process, the change of the phase structure of the NaTiO support establishes a stronger MSI and modified Pt electronic structure, either by charge transfer or through lattice strain. In addition, Cui and co-workers reported that a change in support volume could induce lattice strain on supported Pt catalysts.¹² Accordingly, the volume change of the

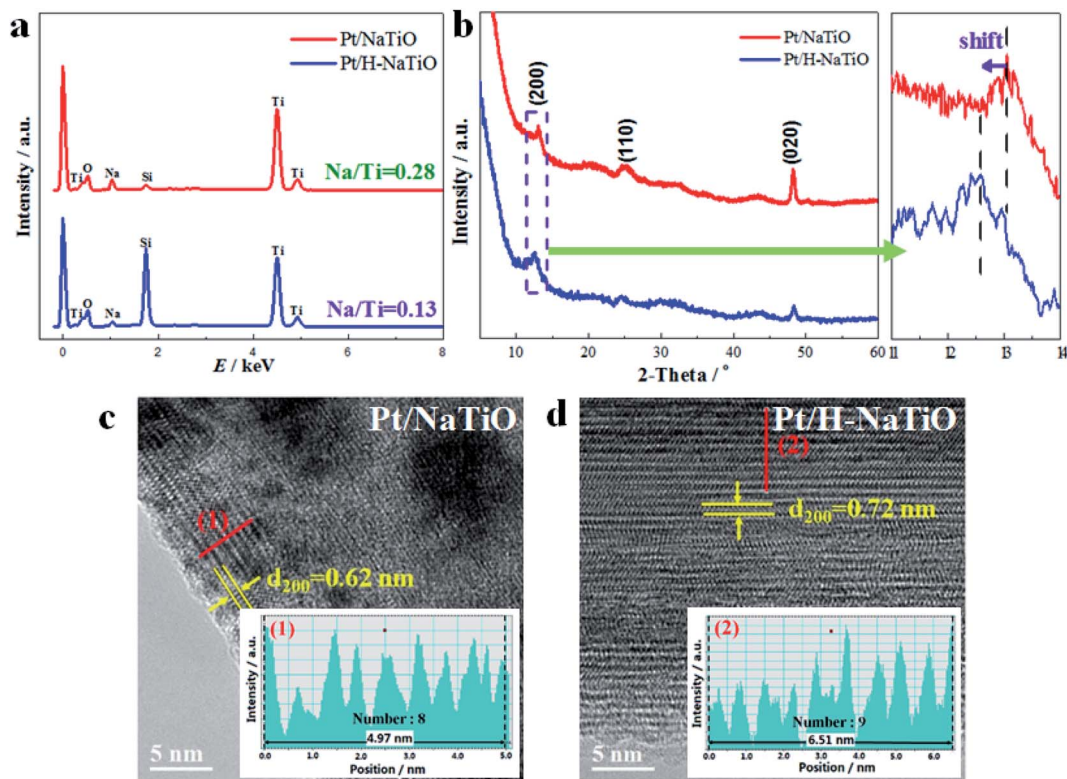


Fig. 5 EDS (a), XRD (b) and HRTEM (c and d) of Pt/NaTiO and Pt/H-NaTiO catalysts.

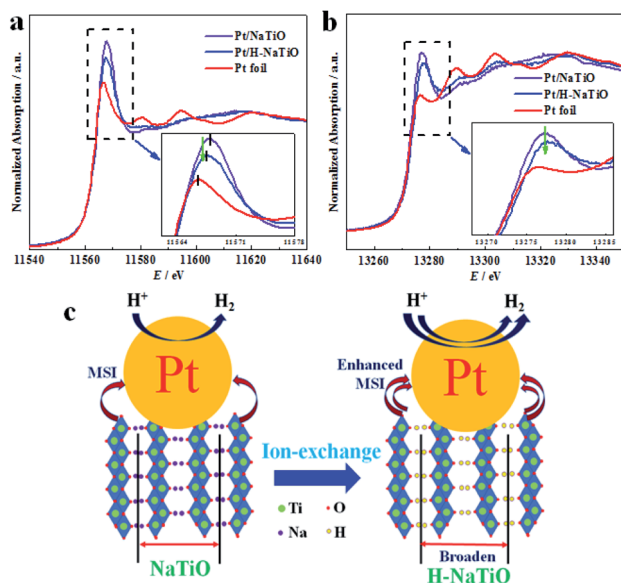


Fig. 6 XANES spectra for Pt L_{3-} (a) and L_{2-} (b) edges for Pt/NaTiO and Pt/H-NaTiO catalysts; schematic of *in situ* enhanced MSI to boost the HER electrocatalytic performance (c).

NaTiO support due to the change of lattice spacing during the ion-exchanging reaction might also give rise to the lattice strain of supported Pt, and in turn facilitate the charge transfer from support to Pt. All these interactions have consequences in terms of the enhanced MSI, which is responsible for the lower

oxidation state of Pt NPs and the higher HER performance in comparison with that of Pt/TiO.

Experimental

Synthesis of TiO and NaTiO nanowires supports

TiO and NaTiO nanowires were prepared *via* a facile hydrothermal process and a subsequent heat treatment similar to our previous work.³⁶ Briefly, 200 mg anatase TiO₂ was transferred into a 50 mL Teflon-lined autoclave with 30 mL of 10 mol L⁻¹ NaOH solution and heated at 150 °C for 24 h. After washing with water and drying for 3 h, the obtained product was then divided into two parts. One was heated at 450 °C for 2 h in air after treated in 0.1 M HClO₄ for 3 h, labeled as TiO support. The other was directly heated at 450 °C for 2 h in air without acidic treatment, named as NaTiO support.

Synthesis of Pt-based catalysts

Pt was deposited on TiO and NaTiO supports by ALD (Savannah 100, Cambridge Nanotechnology Inc., USA) according to our previous report.⁴² The TiO or NaTiO support was placed into a container inside the ALD reactor chamber. High pure N₂ (99.9995%) was used as both a purging gas and carrier gas, and the MeCpPtMe₃ was used as the Pt precursor. To form a steady-state flux of Pt precursor, the container of MeCpPtMe₃ was maintained at 65 °C and the gas lines were held at 150 °C. A 5 s exposure of Pt precursor was used to deposit Pt at 250 °C, and

then the chamber was kept at the vacuum state until it reached room temperature.

Physical characterization

ICP-OES was used to measure the accurate Pt loadings of catalysts. The crystal phases of samples were studied by XRD on a Bruker AXS D8 Advance with a Cu $K\alpha$ radiation. The morphologies of the samples were acquired using a Hitachi S4800 field emission SEM operated at 5 kV equipped with EDS. TEM, HRTEM and HAADF-STEM were performed on the Philips CM12 with a LaB₆ filament. XAS measurements were carried out at the Canadian Light Source (CLS). The Pt L₃ and L₂-edge XANES spectra were collected using the fluorescence yield mode on the hard X-ray microanalysis beamline (HXMA) at the CLS.

Electrochemical measurement

The electrochemical HER measurements were performed in a typical three-electrode electrochemical cell with a glassy carbon rotating-disk electrode as the working electrode. A fresh reversible hydrogen electrode (RHE) and a graphite electrode were respectively used as the reference electrode and the counter electrode. The studied electrolyte was 0.1 M HClO₄ solution. The catalyst ink was prepared by ultrasonically dispersing 2.0 mg catalysts, 2.0 mg XC-72 carbon and 5 μ L Nafion (5 wt%) into 0.4 mL mixture of isopropanol and DI water (4 : 1). 10 μ L of the catalyst ink was drop-casted on the disk electrode (0.196 cm²) to yield a thin film electrode. The HER activity was carried out with a scan rate of 10 mV s⁻¹ at a rotation rate of 1600 rpm. Before recording the HER polarization curves, cyclic voltammetry (CV) between 0.05 V and 1.1 V was performed at a scan rate of 50 mV s⁻¹ to activate the working electrode until a stable plot was achieved. The HER stability was tested by cycling the catalysts from 0 V to -0.3 V for 10 000 cycles at a rotation rate of 1600 rpm.

Conclusions

In summary, a facile and effective strategy aimed at enhancing the MSI between Pt and titanium oxide was successfully developed and validated. We fabricated a Pt catalyst supported on quasi-layered sodium titanate for the HER using ALD. The Pt NP size of approximately 1.5 nm substantially improved the Pt utilization efficiency. The Pt/NaTiO catalyst exhibited considerably higher mass activity (10.3 A mg⁻¹) and long-term stability (95.1%) after 10 000 cycles compared with commercial Pt/C (0.4 A mg⁻¹ and 72.5%). More importantly, the electrocatalytic performance of Pt/NaTiO was obviously superior to that of Pt/TiO₂, which was ascribed to the enhanced MSI. Further study demonstrated that the structural variation of the support due to the ion-exchanging reaction between Na-ions and H-ions in acidic solution was responsible for the enhanced MSI, resulting in further reduction of the Pt oxidation state observed by XAS. The enhancement mechanism was further analyzed and attributed to the change of the charge transfer between Pt and support. This new finding provides an easy and valuable approach to enhance the MSI, which is beneficial for the

development of catalysts with high catalytic performance towards various applications.

Conflicts of interest

There are no conflicts to declare.

Acknowledgements

This work is supported by National Natural Science Foundation of China (Grant No. 21673064, 51802059 and 21905070), China postdoctoral science foundation (Grant No. 2018M631938, 2018T110307 and 2017M621284), Heilongjiang Postdoctoral Fund (LBH-Z17074 and LBH-Z18066), Fundamental Research Funds for the Central Universities (Grant No. HIT. NSRIF. 2019040 and 2019041), Natural Sciences and Engineering Research Council of Canada (NSERC), Canada Research Chair (CRC) Program, Canada Foundation for Innovation (CFI), Canadian Light Source (CLS), Canadian Centre for Electron Microscopy (CEEM) and the University of Western Ontario. Xulei Sui also acknowledges financial support from the China Scholarship Council.

Notes and references

- 1 M. A. Khan, H. Zhao, W. Zou, Z. Chen, W. Cao, J. Fang, J. Xu, L. Zhang and J. Zhang, *Electrochem. Energy Rev.*, 2018, **1**, 483–530.
- 2 Y. Li, Q. Li, H. Wang, L. Zhang, D. P. Wilkinson and J. Zhang, *Electrochem. Energy Rev.*, 2019, **2**, 518–538.
- 3 C. L. Li, H. B. Tan, J. J. Lin, X. L. Luo, S. P. Wang, J. You, Y. H. Kang, Y. Bando, Y. Yamauchi and J. Kim, *Nano Today*, 2018, **21**, 91–105.
- 4 Y. Y. Shao, J. P. Dodelet, G. Wu and P. Zelenay, *Adv. Mater.*, 2019, **31**, 1807615.
- 5 M. Ahmadi, H. Mistry and B. Roldan Cuenya, *J. Phys. Chem. Lett.*, 2016, **7**, 3519–3533.
- 6 L. Zhang, K. Doyle-Davis and X. L. Sun, *Energy Environ. Sci.*, 2019, **12**, 492–517.
- 7 J. Kim, H. E. Kim and H. Lee, *Chemsuschem*, 2018, **11**, 104–113.
- 8 N. Daelman, M. Capdevila-Cortada and N. Lopez, *Nat. Mater.*, 2019, **18**, 1215–1221.
- 9 N. Cheng, L. Zhang, K. Doyle-Davis and X. Sun, *Electrochem. Energy Rev.*, 2019, **2**, 539–573.
- 10 L. Z. Bu, N. Zhang, S. J. Guo, X. Zhang, J. Li, J. L. Yao, T. Wu, G. Lu, J. Y. Ma, D. Su and X. Q. Huang, *Science*, 2016, **354**, 1410–1414.
- 11 P. T. Wang, X. Zhang, J. Zhang, S. Wan, S. J. Guo, G. Lu, J. L. Yao and X. Q. Huang, *Nat. Commun.*, 2017, **8**, 14580.
- 12 H. T. Wang, S. C. Xu, C. Tsai, Y. Z. Li, C. Liu, J. Zhao, Y. Y. Liu, H. Y. Yuan, F. Abild-Pedersen, F. B. Prinz, J. K. Nørskov and Y. Cui, *Science*, 2016, **354**, 1031–1036.
- 13 J. J. Li, Q. Q. Guan, H. Wu, W. Liu, Y. Lin, Z. H. Sun, X. X. Ye, X. S. Zheng, H. B. Pan, J. F. Zhu, S. Chen, W. H. Zhang, S. Q. Wei and J. L. Lu, *J. Am. Chem. Soc.*, 2019, **141**, 14515–14519.

- 14 L. N. Cao, W. Liu, Q. Q. Luo, R. T. Yin, B. Wang, J. Weissenrieder, M. Soldemo, H. Yan, Y. Lin, Z. H. Sun, C. Ma, W. H. Zhang, S. Chen, H. W. Wang, Q. Q. Guan, T. Yao, S. Q. Wei, J. L. Yang and J. L. Lu, *Nature*, 2019, **565**, 631–635.
- 15 G. Pacchioni and H. J. Freund, *Chem. Soc. Rev.*, 2018, **47**, 8474–8502.
- 16 M. Macino, A. J. Barnes, R. Y. Qu, E. K. Gibson, D. J. Morgan, S. J. Freakley, N. Dimitratos, C. J. Kiely, X. Gao, A. M. Beale, D. Bethell, Q. He, M. Sankar, G. J. Hutchings and S. M. Althabhan, *Nat. Catal.*, 2019, **2**, 873–881.
- 17 X. L. Sui, Z. B. Wang, M. Yang, L. Huo, D. M. Gu and G. P. Yin, *J. Power Sources*, 2014, **255**, 43–51.
- 18 Z. H. Weng and F. Zaera, *ACS Catal.*, 2018, **8**, 8513–8524.
- 19 Z. Li, L. Yu, C. Milligan, T. Ma, L. Zhou, Y. R. Cui, Z. Y. Qi, N. Libretto, B. Xu, J. W. Luo, E. Z. Shi, Z. W. Wu, H. L. Xin, W. N. Delgass, J. T. Miller and Y. Wu, *Nat. Commun.*, 2018, **9**, 5258.
- 20 X. L. Sui, C. Z. Li, L. Zhao, Z. B. Wang, D. M. Gu and G. S. Huang, *Int. J. Hydrogen Energy*, 2018, **43**, 5153–5162.
- 21 Y. Chen, S. Ji, W. Sun, Y. Lei, Q. Wang, A. Li, W. Chen, G. Zhou, Z. Zhang, Y. Wang, L. Zheng, Q. Zhang, L. Gu, X. Han, D. Wang and Y. Li, *Angew. Chem., Int. Ed.*, 2020, **59**, 1295–1301.
- 22 T. W. van Deelen, C. Hernández Mejía and K. P. de Jong, *Nat. Catal.*, 2019, **2**, 955–970.
- 23 N. C. Cheng, M. N. Banis, J. Liu, A. Riese, S. C. Mu, R. Y. Li, T. K. Sham and X. L. Sun, *Energy Environ. Sci.*, 2015, **8**, 1450–1455.
- 24 A. M. Karim, V. Prasad, G. Mpourmpakis, W. W. Lonergan, A. I. Frenkel, J. G. Chen and D. G. Vlachos, *J. Am. Chem. Soc.*, 2009, **131**, 12230–12239.
- 25 I. Ro, J. Resasco and P. Christopher, *ACS Catal.*, 2018, **8**, 7368–7387.
- 26 W. Karim, C. Spreafico, A. Kleibert, J. Gobrecht, J. VandeVondele, Y. Ekinici and J. A. van Bokhoven, *Nature*, 2017, **541**, 68–71.
- 27 A. R. Puigdollers, P. Schlexer, S. Tosoni and G. Pacchioni, *ACS Catal.*, 2017, **7**, 6493–6513.
- 28 H. Ha, S. Yoon, K. An and H. Y. Kim, *ACS Catal.*, 2018, **8**, 11491–11501.
- 29 W. Zhan, Q. He, X. Liu, Y. Guo, Y. Wang, L. Wang, Y. Guo, A. Y. Borisevich, J. Zhang, G. Lu and S. Dai, *J. Am. Chem. Soc.*, 2016, **138**, 16130–16139.
- 30 L. Wang, J. Zhang, Y. Zhu, S. Xu, C. Wang, C. Bian, X. Meng and F.-S. Xiao, *ACS Catal.*, 2017, **7**, 7461–7465.
- 31 A. M. Ganzler, M. Casapu, P. Vernoux, S. Loridant, F. Aires, T. Epicier, B. Betz, R. Hoyer and J. D. Grunwaldt, *Angew. Chem., Int. Ed.*, 2017, **56**, 13078–13082.
- 32 H. L. Tang, Y. Su, B. S. Zhang, A. F. Lee, M. A. Isaacs, K. Wilson, L. Li, Y. G. Ren, J. H. Huang, M. Haruta, B. T. Qiao, X. Liu, C. Z. Jin, D. S. Su, J. H. Wang and T. Zhang, *Sci. Adv.*, 2017, **3**, 10.
- 33 J. J. Gao, P. Du, Q. H. Zhang, X. Shen, F. K. Chiang, Y. R. Wen, X. Lin, X. J. Liu and H. J. Qiu, *Electrochim. Acta*, 2019, **297**, 155–162.
- 34 P. S. M. Kumar, V. K. Ponnusamy, K. R. Deepthi, G. Kumar, A. Pugazhendhi, H. Abe, S. Thiripuranthagan, U. Pal and S. K. Krishnan, *J. Mater. Chem. A*, 2018, **6**, 23435–23444.
- 35 X. L. Sui, Z. B. Wang, C. Z. Li, J. J. Zhang, L. Zhao, D. M. Gu and S. Gu, *J. Mater. Chem. A*, 2015, **3**, 840–846.
- 36 X. L. Sui, Z. B. Wang, C. Z. Li, J. J. Zhang, L. Zhao and D. M. Gu, *J. Power Sources*, 2014, **272**, 196–202.
- 37 L. F. Que, F. D. Yu, L. L. Zheng, Z. B. Wang and D. M. Gu, *Nano Energy*, 2018, **45**, 337–345.
- 38 L. F. Que, F. D. Yu, X. L. Sui, L. Zhao, J. G. Zhou, D. M. Gu and Z. B. Wang, *Nano Energy*, 2019, **59**, 17–25.
- 39 Y. Gao, Z. C. Xiao, D. B. Kong, R. Iqbal, Q. H. Yang and L. J. Zhi, *Nano Energy*, 2019, **64**, 103879.
- 40 C. T. Hsieh, X. F. Chuah, C. L. Huang, H. W. Lin, Y. A. Chen and S. Y. Lu, *Small Methods*, 2019, **3**, 1900234.
- 41 S. L. Jiao, Z. Y. Yao, F. Xue, Y. F. Lu, M. C. Liu, H. Q. Deng, X. F. Ma, Z. X. Liu, C. Ma, H. W. Huang, S. C. Ruan and Y. J. Zeng, *Appl. Catal., B*, 2019, **258**, 117964.
- 42 N. C. Cheng, S. Stambula, D. Wang, M. N. Banis, J. Liu, A. Riese, B. W. Xiao, R. Y. Li, T. K. Sham, L. M. Liu, G. A. Botton and X. L. Sun, *Nat. Commun.*, 2016, **7**, 13638.
- 43 S. J. Tauster, S. C. Fung and R. L. Garten, *J. Am. Chem. Soc.*, 1978, **100**, 170–175.
- 44 A. Lewera, L. Timperman, A. Roguska and N. Alonso-Vante, *J. Phys. Chem. C*, 2011, **115**, 20153–20159.